ADVANCED OPTICAL MATERIALS
www.advopticalmat.de

Light-Induced Ferroelectric Modulation of p-n Homojunctions in Monolayer MoS_2

Mariola O Ramirez, Jaime Fernandez-Tejedor, Daniel Gallego, Javier Fernández-Martinez, Pablo Molina, David Hernández-Pinilla, Julio Gómez-Herrero, Pablo Ares, and Luisa E. Bausá*

The association of 2D materials and ferroelectrics offers a promising approach to tune the optoelectronic properties of atomically thin Transition Metal Dichalcogenides (TMDs). In this work, the combined effect of ferroelectricity and light on the optoelectronic properties of monolayer (1L)-MoS_2 deposited on periodically poled lithium niobate crystals is explored. Using scanning micro-photoluminescence, the effect of excitation intensity, scanning direction, and domain walls on the 1L-MoS_2 photoluminescence properties is analyzed, offering insights into charge modulation of MoS_2. The findings unveil a photoinduced charging process dependent on the ferroelectric domain orientation, in which light induces charge generation and transfer at the monolayer-substrate interface. This highlights the substantial role of light excitation in ferroelectrically-driven electrostatic doping in MoS_2. Additionally, the work provides insights into the effect of the strong, nanometrically confined electric fields on $LiNbO_3$ domain wall surfaces, demonstrating precise control over charge carriers in MoS_2, and enabling the creation of deterministic p-n homojunctions with exceptional precision. The results suggest prospects for novel optoelectronic and photonic application involving monolayer TMDs by combining light-matter interaction processes and the surface selectivity provided by ferroelectric domain structures.

1. Introduction

In the last years, Transition Metal Dichalcogenides (TMDs) -based p-n junctions have been extensively studied and a variety of prototypes such as light-emitting diodes, photodetectors, or photovoltaic devices have been developed.[1–5] TMDs-based p-n junctions are usually produced in the form of vertical (out-of-plane) heterostructures by stacking face to face two different TMD materials with opposite charge carriers such as p-WS_2 and n-MoS_2.[6,7] The construction of lateral (in-plane) p-n heterojunctions has also been reported. In this case the deterministic transfer method cannot be easily applied, and different bottom-up fabrication methods should be employed.[8–10] Of particular relevance in designing novel electronic and optoelectronic devices are TMD-based p-n homojunctions. In these systems, perfect lattice matching, continuous band bending, and efficient charge transfer are highly beneficial for carrier transport and separation at the junction. In fact, improved rectifying features, more efficient photoresponses, and a better carrier mobility compared to TMDs-based lateral heterojunctions have been reported.[11] The different strategies employed to create TMDs-based p-n homojunctions include thickness modulation in ambipolar materials,[12,13] chemical doping by substitution, intercalation, or surface modulation,[14–16] and electrostatic doping in which gate voltages are applied to modulate the type and carrier concentration at different spatial regions.[2,4,5] Recently, the possibility of using ferroelectric substrates to modulate the carrier type in TMDs has been also demonstrated enabling the formation of lateral p-n homojunctions without the need of external gating.[17–21] However, while the electrical properties of these systems have been extensively studied in previous works, the optical features of p-n homojunctions have not received much attention, and there has been limited research on how TMDs photoluminescence (PL) is modulated at the interfaces of these junctions.[22,23]

It is well established that single layer 1L-TMDs emit light much more efficiently than multi-layer structures due to the layer dependent indirect-to-direct band gap transition. In addition, the

M. O Ramirez, J. Fernandez-Tejedor, J. Fernández-Martinez, P. Molina, D. Hernández-Pinilla, L. E. Bausá
Dept. Física de Materiales
Universidad Autónoma de Madrid
Madrid 28049, Spain
E-mail: mariola.ramirez@uam.es

M. O Ramirez, J. Fernandez-Tejedor, D. Gallego, J. Fernández-Martinez, P. Molina, D. Hernández-Pinilla, J. Gómez-Herrero, P. Ares, L. E. Bausá
Instituto Nicolás Cabrera
Universidad Autónoma de Madrid
Madrid 28049, Spain

M. O Ramirez, D. Gallego, J. Gómez-Herrero, P. Ares, L. E. Bausá
Condensed Matter Physics Center (IFIMAC)
Universidad Autónoma de Madrid
Madrid 28049, Spain

D. Gallego, J. Gómez-Herrero, P. Ares
Dept. Física de la Materia Condensada
Universidad Autónoma de Madrid
Madrid 28049, Spain

The ORCID identification number(s) for the author(s) of this article can be found under https://doi.org/10.1002/adom.202400624

DOI: 10.1002/adom.202400624

atomic thickness nature of 1L-TMDs offers a unique opportunity to modulate their optoelectronic properties by means of the surrounding environment.[24] In particular, the association of TMDs with ferroelectrics has recently emerged as a promising approach for fabricating reconfigurable and nonvolatile 2D devices with diverse optoelectronic applications.[17–19] However, most of them are based on multilayer structures which hampers their PL characterization. In this context, the ability to optically address the formation of 1L-TMD-based lateral p-n junctions on ferroelectric domain structures provides a simple tool to characterize the device without the need for external electrodes, whose fabrication is a recognized challenge in TMD device research.[25–27] Moreover, the PL analysis provides fundamental insights on the influence of the strong electric fields nanometrically confined on ferroelectric domain walls on photogenerated neutral and charged excitons (trions). Such insights may have technological implications for optoelectronics, nanophotonics, and quantum optics.

In this work, a periodically poled $LiNbO_3$, one of the most versatile and attractive current platforms for integrated photonics,[28,29] is used as ferroelectric substrate for 1L-MoS_2. The modulation of the carrier density induced by the ferroelectric domain pattern in 1L-MoS_2 is studied on both types of domains, P_{up} and P_{down} revealing the formation of p-n homojunctions. While previous studies have exploited the association of 2D materials on $LiNbO_3$ ferroelectric substrates from different perspectives,[30–34] several aspects such as the influence of the strongly confined electric fields at the domain walls or the combined effect of photodoping and ferroelectricity remains unexplored. Here, we use spatially resolved scanning micro-PL at different excitation power values to systematically investigate how the excitation intensity, excitation scanning direction, and domain walls influence the PL properties of 1L-MoS_2. This approach yields new knowledge into charge modulation of 1L-MoS_2 on domain surfaces and walls.

The work is organized as follows. On the one hand, we analyze the combined effect of both ferroelectricity and photodoping on 1L-MoS_2. The results highlight the presence of a domain-dependent photodoping associated with charge creation and transfer at the monolayer-substrate interface, pointing out the major role of light excitation in ferroelectrically driven electrostatic doping in MoS_2. On the other hand, an in-depth analysis of the influence of domain walls on the electronic properties of 1L-MoS_2 is carried out. At low excitation intensities, we observe an abrupt modification in the charge carrier concentration of 1L-MoS_2 in the vicinities of the domain walls, which relates to the presence of a nanometrically confined electric field at the domain wall surfaces of $LiNbO_3$ crystals.[35,36] The results demonstrate that domain walls can offer precise nanometric control over charge carriers, generating deterministic p-n regions on 1L-MoS_2 with exceptional precision. Moreover, the formation of lateral p-n homojunctions confined at the proximities of domain walls is confirmed by electrical measurements showing a clear rectifying behavior consistent with the local carrier density modulation of 1L-MoS_2 in the proximities of the domain wall. Lastly, we demonstrate the possibility of an optically driven modulation of the potential barrier heights in the MoS_2 p-n homojunctions defined on the ferroelectric domain walls. Specifically, we observe an alternating reduction and enhancement of the 1L-MoS_2 PL across successive domain walls. This modulation exhibits a directional dependence on the excitation scanning direction, enabling a switchable spatial redistribution of the PL intensity at the junctions when the laser scanning direction is reversed. The results are interpreted in terms of a light-driven modulation of the potential barrier heights at consecutive p-n junctions induced by charge separation and accumulation effects.

Our study emphasizes the usefulness of spatially resolved scanning PL spectroscopy as an efficient way to investigate the formation of p-n junctions and their performance during above bandgap illumination in 1L-TMDs. Additionally, the demonstration of spatially confined ferroelectrically induced p-n homojunctions in 1L-MoS_2 provides a promising approach for the simple fabrication of reconfigurable devices for photodetection and other photonic applications.

2. Results and Discussion

Figure 1a displays the optical micrograph of a mechanically exfoliated MoS_2 flake deterministically transferred to the polished surface of a periodically poled $LiNbO_3$ ferroelectric crystal. The width of the alternating ferroelectric domains is ≈11 µm, more than one order of magnitude larger than the spatial resolution of our scanning µ-PL experiments. Figure 1b shows the differential micro-reflectance spectra of the MoS_2 flake recorded on the 1L region. The energy resonances in the spectra, located at ≈655, 600, and 455 nm, correspond to the A, B, and C excitonic transitions of MoS_2, respectively. The measured exciton energies and relative intensities are in good agreement with previously reported results for 1L-MoS_2.[37,38] For comparison, the reflectance of the 2L-MoS2 region is also shown. Consistent with prior studies,[38,39] the positions of the C and A-excitons show a redshift as the number of layers increases, while the B-exciton does not shift. This behavior can be explained by two main effects: the redshift in the band-to-band absorption edge and the decrease in excitonic binding energy as the material undergoes from 1L to 2L. In the case of the A-exciton the first effect is dominant resulting in a clear redshift. Conversely, for the B-exciton the second effect dominates, which justifies the experimental observation.[40]

The position of these bands shows a spectral red shift as the number of layers increases. The obtained exciton energies and relative intensities agree well with previously reported results for 1L-MoS_2.[38] The reflectance of the 2L-MoS_2 region is also shown for the sake of comparison. Figure 1c shows the micro-reflectance spectra of 1L-MoS_2 on two opposite polarity ferroelectric domains, P_{up} and P_{down}. While the intensity of the C band remains basically the same regardless of the domain orientation, slight modifications of the intensities of the A and B excitonic emissions are observed when comparing the spectra on each domain. These results are consistent with the response of the involved transitions to doping effects. As reported, the intensity of the A and B excitonic transitions varies with doping levels, while the intensity of the C band remains almost unaffected.[37] In particular, a reduction of the A and B intensities of ≈3% on the P_{up} domain with respect to that on the P_{down} domain is observed. A small redshift (≈4.5 meV) in the region of the A exciton is also detected on P_{up} domains as highlighted in Figure 1d. This slight spectral change could be related to a higher presence of trions on the positive P_{up} domain compared to the negative P_{down}

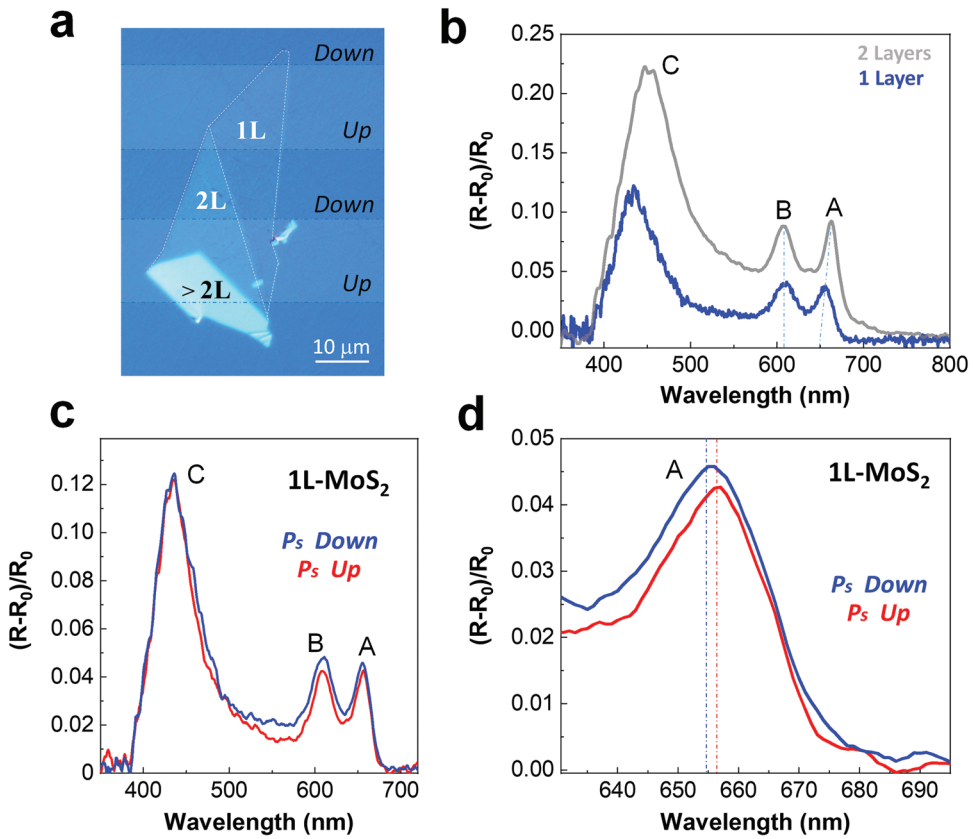

Figure 1. Fabrication and characterization of 1L-MoS_2-$LiNbO_3$. a) Optical image of a mechanically exfoliated MoS_2 flake transferred onto the surface of a periodically poled $LiNbO_3$ crystal; the contrast between different polarized domains in the image is highlighted using false-color imaging. The number of MoS_2 layers and the orientation of the ferroelectric polarization are indicated. b) Micro-reflectance spectra in a bilayer (blue) and a monolayer (gray) region of the MoS_2 flake. The spectral positions of the A, B, and C excitons are indicated. c) Micro-reflectance spectra of 1L-MoS_2 on P_{down} (blue) and P_{up} (red) ferroelectric domains. d) Detail of the micro-reflectance spectra of 1L-MoS_2 around the A exciton spectral region.

domain, which suggests the presence of ferroelectrically-induced electronic doping in the system.

Further information on the spatial modulation of the carrier density produced by the ferroelectric domain pattern can be obtained by analyzing the PL signal of the 1L-MoS_2 on P_{up} and P_{down} ferroelectric domains when varying the excitation intensity. **Figure** 2a shows the optical image of the 1L-MoS_2 deposited on the ferroelectric domain structure together with the spatial distribution of the PL intensity obtained by integrating the emission spectra around the A exciton band. The excitation intensity was $2{\cdot}10^5$ W cm^{-2}. As observed, the change in the spontaneous polarization orientation of the ferroelectric substrate is correlated to a strong modulation of the 1L-MoS_2 PL with maximum values occurring on the P_{down} domains. The spectra of 1L-MoS_2 on each type of domain, P_{down} and P_{up}, are compared in Figure 2b. They both show an asymmetric shape due to the contribution of two resonances labeled as A and A^- in the figure. The A peak corresponds to the neutral exciton emission centered at ≈655 nm. The A^- band centered at ≈670 m is associated with the presence of trions. As established, the ratio of exciton/trion emission in 1L-MoS_2 is determined by the carrier concentration density in the layer.[14] In fact, the charge balance at the 1L-MoS_2-$LiNbO_3$ interface produces a *p*-type doping on the P_{down} domain, which leads to a predominant emission from neutral excitons from that domain. Conversely, the P_{up} domain surface induces an *n*-type doping, which quenches the exciton emission and therefore increases the trion spectral weight in the PL spectrum. On this domain, the total emitted intensity decreases due to the lower quantum yield of trions at room temperature compared to that of neutral excitons.[41] The observed PL contrast is in good agreement with previous works[22,23,32] and indeed, it can also be correlated to previous results obtained by electrostatic doping in MoS_2 in the voltage range −50 to +50 V,[42] verifying the effective doping and the spatial carrier density modulation induced in 1L-MoS_2 by the ferroelectric domain patterning of a $LiNbO_3$ substrate. An opposite contrast in PL to that observed in this work has been reported,[43] which could be attributed to a more complex sample preparation that could modify the balance between the polarization charge and the screening charge, and therefore the doping of MoS_2.

Figure 2c shows, as an example, the deconvolution of the PL into the exciton (A) and trion (A^-) bands on two ferroelectric domains of opposite polarity. Through the PL intensity weight of both resonances, and using the expression derived by Mouri et al.,[14] it is possible to extract quantitative information on the doping concentration of 1L-MoS_2 on each type of domain. By considering the mass action law associated with trions and assuming that the radiative decay rate of excitons and trions varies in the

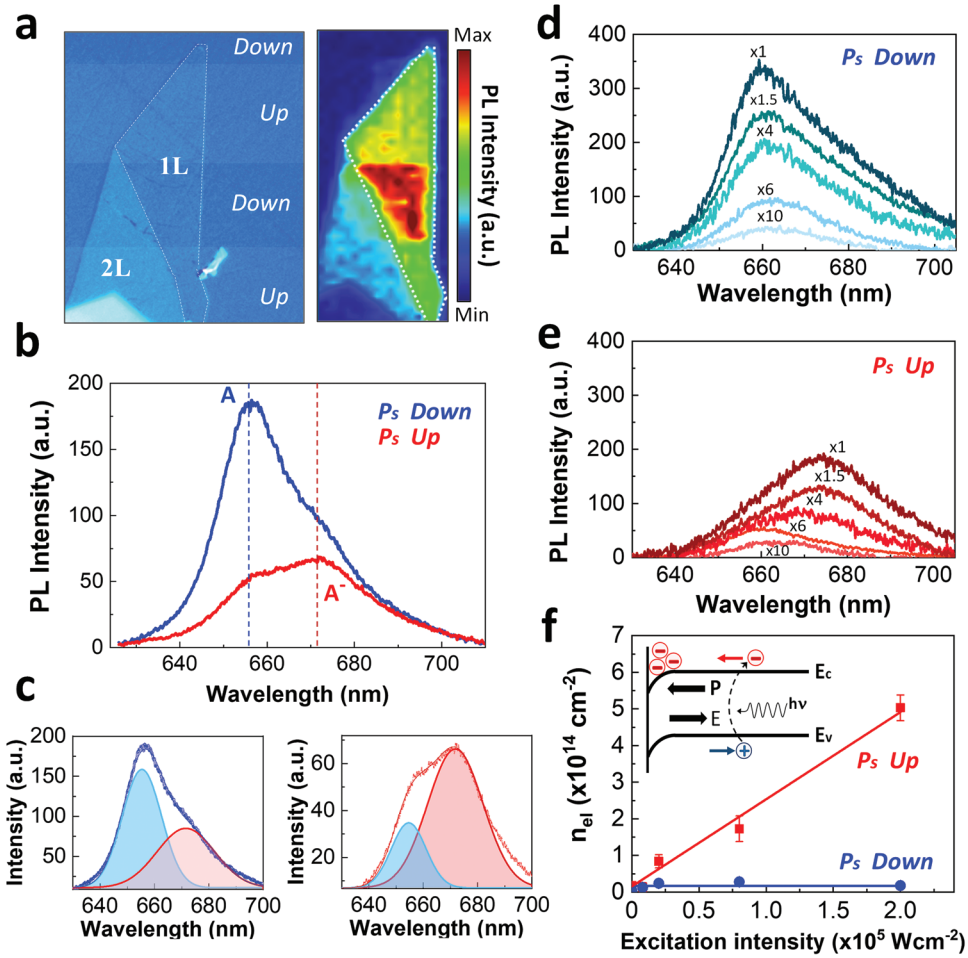

Figure 2. Domain-dependent photoinduced charging process. a) Spatial distribution of the integrated PL intensity of 1L-MoS_2 on $LiNbO_3$ (right) and the corresponding optical image (left); the contrast between different polarized domains in the image is highlighted using false-color imaging. The excitation intensity was fixed at $2{\cdot}10^5$ W cm^{-2}. b) PL spectra of 1L-MoS_2 on P_{down} (blue) and P_{up} (red) ferroelectric domains. The spectral positions of the exciton (A) and trion (A^-) bands are indicated. c) Deconvoluted spectra by the exciton (shadowed blue) and trion (shadowed red) contributions to 1L-MoS_2 PL on the P_{down} (left) and P_{up} (right) domains. d,e) Evolution of 1L-MoS_2 PL spectra in the 10^3–10^5 W cm^{-2} range of excitation intensity recorded on the P_{down} and P_{up} domains, respectively. For the sake of comparison, the spectra have been rescaled according to the factors displayed in the panels. f) Estimated electron density of 1L-$iMoS_2$ on P_{up} (red) and P_{down} (blue) domains as a function of the excitation intensity. The inset shows a schematics of the band bending and photo-doping process on the P_{up} domain surface. Adapted from Ref. [46].

same proportion, the electron density concentration, n_{el}, can be derived from the equation:[14]

$$\frac{I_{tri}}{I_{total}} = \frac{\frac{\gamma_{tri}}{\gamma_{ex}} \times \frac{N_{tri}}{N_{ex}}}{1 + \frac{\gamma_{tri}}{\gamma_{ex}} \times \frac{N_{tri}}{N_{ex}}} \sim \frac{4 \times 10^{-14} n_{el}\ [\mathrm{cm}^{-2}]}{1 + 4 \times 10^{-14} n_{el}\ [\mathrm{cm}^{-2}]} \quad (1)$$

where γ_{ex} and γ_{tri} are the radiative decay rate of exciton and trions, respectively, with $\gamma_{ex}/\gamma_{tri} \approx 20/3$,[14] and N_{tri} and N_{ex} account for the population of excitons and trions derived from the steady-state solutions. According to Equation (1), the estimated electron density is around five times higher on the P_{up} domain (n_{el} ~$8.2{\cdot}10^{13}$ cm^{-2}) than on the P_{down} domain (n_{el} ~$1.6{\cdot}10^{13}$ cm^{-2}), the difference of electron density being $\Delta n_{el} = 6.6{\cdot}10^{13}$ cm^{-2}. However, this estimated carrier concentration and the strong spectral differences observed on both domains cannot be completely attributed to ferroelectric doping. Rather, the effect of photodoping should be also considered, and in fact, the impact of photodoping is particularly relevant at high excitation power altering the carrier concentration in TMDs and thus, the interplay between exciton and trions.[44,45]

To investigate the combined influence of the substrate spontaneous polarization and photodoping on 1L-MoS_2, the PL spectra on the surface of each type of ferroelectric domain have been recorded in the 10^3–10^5 W cm^{-2} range of excitation intensity. As observed, in Figure 2d,e, for the lowest intensities, the PL spectra are similar on both P_{down} and P_{up} domains suggesting a negligible difference of charge carrier density, and therefore, a minor contribution of the ferroelectric doping at the minimal incident intensity. However, for incident intensities exceeding 10^4 W cm^{-2}, the PL spectra on each domain exhibit significant differences. While on the P_{down} region the spectra are governed by the A excitonic transition, on the P_{up} domain, the trion contribution dominates the emission, resulting in a redshift of the overall

PL. This spectral dependence on the incident excitation intensity is a characteristic signature of a photoinduced electron charging process (photodoping), which is associated with charge creation and transfer at the monolayer-substrate interface.[44,45] Possible thermal effects could also be considered to account for the spectral changes observed at the higher excitation intensities. However, the exciton energy position does not show any detectable redshift with increasing excitation power that could be related to a temperature increase,[47] which points to photodoping as the dominant factor responsible for the observed changes in PL.

Figure 2f presents an estimation of the electronic density on the P_{up} and P_{down} domains as a function of the excitation intensity obtained from the exciton and trion spectral contributions using Equation (1). The growth rate of the electron density strongly depends on the polarization orientation, with a higher rate observed on the P_{up} domain. This result clearly reveals the presence of a domain-dependent photodoping process in 1L-MoS_2 deposited on $LiNbO_3$, according to the interface charges of each type of ferroelectric domain surface. In fact, the underlying mechanism can be associated with induced free carriers and the presence of a polarization-dependent band bending at the polar surface of the ferroelectric crystal as established by a variety of photo-assisted processes in this material.[48–51] The domain-dependent band bending (upward and downward in the P_{down} and P_{up} domains, respectively) results in an electric field at the ferroelectric surfaces that facilitates charge separation and transfer at the $LiNbO_3$-MoS_2 interface. In particular, this band bending produces the accumulation of photo-excited electrons on the surface of P_{up} domains favoring the dominant presence of negative charged excitons (trions). See inset in Figure 2f. It also explains the constant behavior of the electronic density observed on the P_{down} domain as the excitation light intensity is increased. Accordingly, light-induced p-n homojunctions can be formed in 1L-MoS_2 deposited on alternate domain structures in $LiNbO_3$. The results show the crucial influence of light excitation in ferroelectrically driven doping. In fact, the role of $LiNbO_3$ as ferroelectric substrate to spatially modulate the carrier density in MoS_2 is clearly manifested under light excitation. We have confirmed that photodoping with high excitation intensity lasts at least for several weeks. On the other hand, as observed in Figure 2f, the difference between the electronic density on each type of domain approaches zero in the absence of excitation light, which indicates a minor contribution of the spontaneous polarization itself on the doping modulation of MoS_2. Indeed, the values of the electronic density obtained at the y- axis intercept by a least square fitting of the linear relationship in Figure 2f ($n_{el} \sim 10^{13}$ cm^{-2}) are in the order of those reported for pristine 1L-MoS_2.

The results in Figure 2 refer to effects on the 1L-MoS_2 on the domain surfaces. However, for a comprehensive view, the influence of the domain wall surfaces on the electronic properties of 1L-MoS_2 should be also considered. As previously established, a non-uniform electric field distribution is present on the surface of ferroelectric domain patterns in $LiNbO_3$.[35,36] This field distribution shows a strong out-of-plane field z-component at the domain walls surfaces due to the antiparallel ferroelectric domain structure. This field component has been calculated to be ≈0.5 MVm^{-1}, ten times larger than that on the domain surfaces, and changes its sign in the proximity of the domain wall from one domain to another.[35,36] Therefore, considering that this electric field values are comparable to those obtained with a split gate configuration, it is worth addressing here the impact of the strong nanometrically-confined field at the domain walls surfaces on the optical and electronic properties of 1L-MoS_2. To that aim, we have analyzed the behavior of the 1L-MoS_2 PL on the vicinity of a domain wall for a much lower excitation intensity (≈10^3 W cm^{-2}). **Figure 3** shows the PL obtained in a narrow spatial region around a domain wall with a step precision that corresponds to the limit of the spatial resolution of our experimental setup. The integrated emission intensity is displayed in Figure 3a. Four different regions can be distinguished (zone I to IV). The PL intensity on both domain surfaces P_{down} and P_{up} (zone I and IV, respectively) are comparable since photodoping effects on the domain surfaces can be neglected at the employed excitation power. However, in the vicinity of the domain wall, a singularity is observed, featuring a sharp increase of the emitted intensity (zone II) followed by a decrease (zone III). This singularity can be related to the strong values of the electric field distribution on the domain wall surface. The spectra obtained in the different regions are shown in Figure 3b. On the P_{down} and P_{up} domains (region I and IV, respectively) a similar spectral shape, consistent with the low electrostatic doping displayed at low excitation intensities, is observed (see Figure 2). However, on zones II and III the PL exhibits significant changes, indicating a clear difference in the electronic doping between those zones. Zone II shows a dominant contribution of excitons (*p*-type doping), while zone III reveals a higher relative contribution of trions (*n*-type doping). The observed spectral changes indicate an abrupt modulation of the charge carrier concentration on 1L-MoS_2 on the proximity of the domain wall. In fact, the results reveal that, for low excitation intensity, the modulation of the electronic doping primarily occurs on the vicinity of the domain walls, rather than on the domain wall surfaces. Here we note that similar PL features are observed in the vicinity of consecutive domain walls when sequentially scanning several domains. Therefore, at low excitation intensity, the domain walls features provide nanometric control of charge carriers, generating deterministic and precise nanometric p-n homojunctions. The narrow spatial region where the singularity is observed agrees with the ultranarrow width of the domain walls. While these are typically nanometer-wide regions, the impact of the strong out-of-plane electric field, which extends into the domain surface region, combined with our diffraction-limited lateral spatial resolution, accounts for the observed spatial extension along the domain wall.

To corroborate the optical results, we measured current-voltage (I-V) curves by using two AFM cantilevers with platinum-coated nanometer-radius tips in contact with the 1L-MoS_2 *i)* on a single domain region, and *ii)* on both sides of a ferroelectric domain wall where the p-n junction is formed. The results are shown in Figure 3c. While for the case of the single domain region an almost linear behavior is obtained, a clear diode-like rectifying behavior is detected across the p-n junction. This result, obtained in the absence of excitation light, and therefore, with a negligible doping difference between domains, verifies the presence of a noticeable electrostatic doping associated with the presence of the out-of-plane electric field in the proximities of the domain wall surface. Figure S1 in the Supplementary Section shows additional I-V curves collected on domain surfaces for several 1L-MoS_2 monolayers transferred on periodically poled $LiNbO_3$

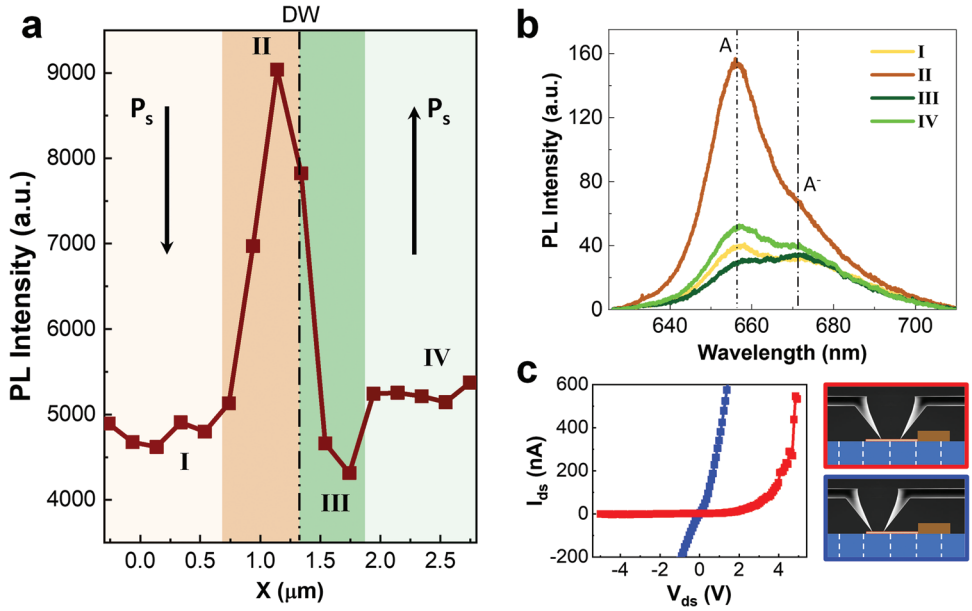

Figure 3. Nanometric control over charge carriers in MoS_2. a) Integrated PL intensity of 1L-MoS_2 on the vicinity of a ferroelectric domain wall in $LiNbO_3$ for an excitation intensity close to 10^3 W cm^{-2}. b) PL spectra of 1L-MoS_2 in different regions: I and IV correspond to the P_{down} and P_{up} domain surfaces, respectively; II and III correspond to the vicinities of the domain wall surfaces. The spectral positions of the exciton (A) and trion (A^-) bands are indicated. c) Dark intensity-voltage (I–V) curves measured contacting the 1L-MoS_2 by using two Pt-coated tips on a same single domain surface (blue) and both sides of a single domain wall (red). Schematics of the experimental configuration are shown in the right panels.

substrates. They all exhibit a similar behavior without any rectification, consistent with the minor contribution of the spontaneous polarization itself on the doping modulation of MoS_2.

Finally, the impact of both electrostatic and photodoping effects on the charge carrier modulation was evaluated by scanning two consecutive junctions (domain walls) at an intermediate excitation intensity (≈10^4 W cm^{-2}). To record this larger spatial region, a larger step size than that of Figure 3 was used, which resulted in a lower spatial resolution. **Figure** 4a displays the PL spatial map recorded upon these experimental conditions, scanning the domains from left to right. As seen, increasing the incident laser intensity results into a drastic PL spatial redistribution when scanning consecutive domains. Namely, the PL intensity decreases when crossing the first junction and increases at the second one. This alternating PL reduction and enhancement of 1L-MoS_2 across successive ferroelectric domain walls (n-p and p-n homojunctions) is clearly visible in the spatial profiles displayed in Figure 4b. Both profiles were registered under the same experimental conditions but reversing the scanning direction from right to left. The results show that in both cases the PL intensity decreases when crossing the first junction and increases on the second one, irrespective of the scanning direction. This leads to a directional switchable redistribution of the emitted light on consecutive junctions. The schemes in Figure 4c explain the PL behavior. When the first n-p junction is optically excited, a relatively large number of excitons are generated. The presence of the built-in electric field at the depletion region of the junction causes dissociation of part of the photogenerated excitons, driving electrons into the *n*-type region and holes into the *p*-type. This results in a reversed bias of the first barrier and a PL decrease. This fact, together with the continuous illumination along the P_{down} domain during the scanning process results in a charge accumulation that biases the second junction forward favoring the radiative recombination and the enhancement of the emission. Moreover, because of photodoping, the electron density on the P_{up} domain is substantially increased (see Figure 2f), and therefore, its *n*-type character, which enlarges the potential barrier height at the first junction (reversed bias) and the efficiency of electron-hole dissociation. The separation of carriers (electrons and holes) affects the equilibrium of the homojunctions leading to the increase and enlargement of the lateral depletion region. Similar photoexcited charge dynamics have been observed for lateral Schottky barriers using scanning photocurrent microscopy.[52]

Figure 4d depicts a series of profiles recorded when scanning the 1L-MoS_2 on three consecutive domains from left to right for laser intensities ranging from 10^2 to 10^5 W cm^{-2}. At low excitation intensities (blue), in the order of 10^2 W cm^{-2}, photodoping does not play a major role, the similarity in the spectral shapes on both domains and the singularities at domain walls agree with Figure 3. At higher excitation intensities (green), the photodoping effect becomes important, increasing the built-in field at the first scanned barrier, and the efficiency of electron-hole dissociation. The separation of carriers (electrons and holes) affects the equilibrium of the homojunctions leading to the increase and enlargement of the first potential barrier. The positive photogenerated carriers are driven to the second junction, weakening the potential barrier, which favors their radiative recombination. Finally, at the highest excitation intensities (red) (≈10^5 W cm^{-2}), the polarization-dependent photodoping governs the scenario, and the large number of carriers generated on the domain surface dominates and masks the effects on the domain walls. This results in a homogeneous spatial dependence of the emitted intensity for both *p*- and *n*-type doped MoS_2.

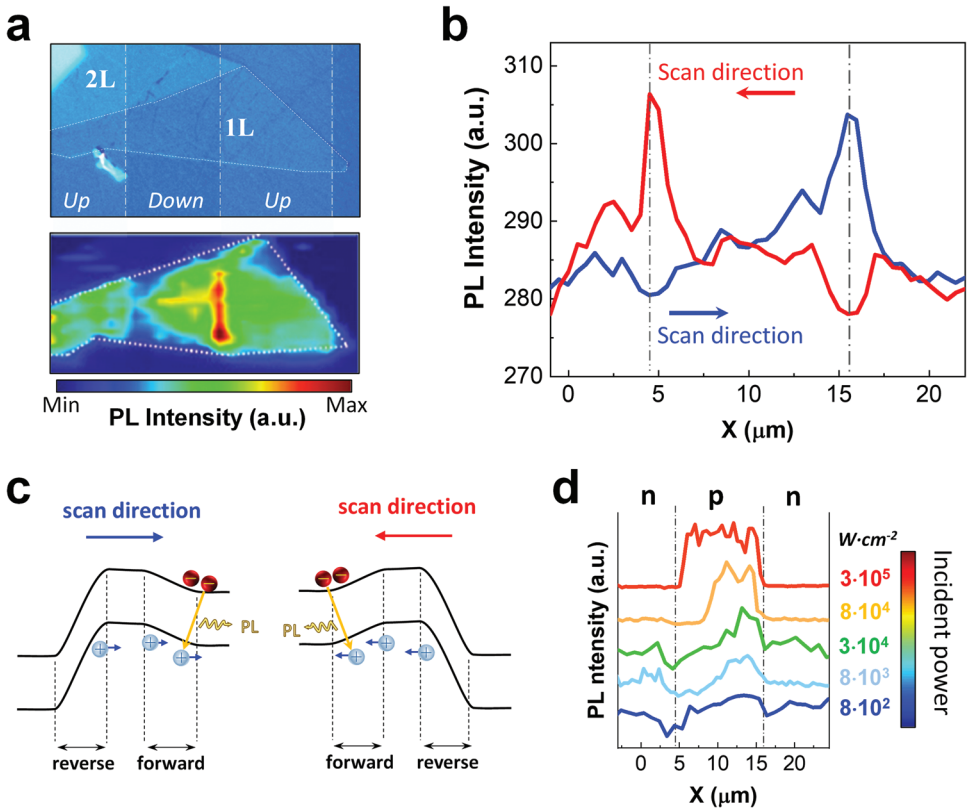

Figure 4. Light-driven modulation of potential barrier heights. a) Spatial distribution of the integrated PL intensity of 1L-MoS_2 on $LiNbO_3$ (bottom) and the corresponding optical image (top). The excitation power was 10^4 W cm^{-2} and the scanning from left to right. b) Spatial profiles of the integrated MoS_2 PL intensity obtained by scanning along two opposite directions. Dashed-dotted lines indicate the position of the domain walls. c) Proposed mechanism explaining the observed spatial distribution of PL. Schematics of the energy bands and diffusion of charge carriers are shown for the two PL scanning directions. d) Spatial profiles of the integrated PL of 1L-MoS_2 along three consecutive domains for laser intensities in the 10^2–10^5 W cm^{-2} range. For illustrative purposes the profiles have been normalized and vertically translated. The scanning direction in this case is from left to right.

3. Summary and Conclusion

To summarize, we have shown the usefulness of spatially resolved scanning PL spectroscopy as an efficient way to investigate the formation of lateral p-n junctions and their performance during above bandgap illumination in 1L-TMDs. In addition to direct imaging and probing of the lateral homojunctions without the need for external electrodes, we have performed detailed spectroscopic studies as a function of the incident laser intensity to evaluate the interplay between excitons and trions in monolayer MoS_2. We found that while at high incident powers ($\approx 10^5$ W cm^{-2}) the ferroelectric polarization-dependent photodoping process favors the modulation of charge carriers on the surface of P_{up} and P_{down} domains, at much lower incident powers ($\approx 10^3$ W cm^{-2}) the spatial carrier density modulation in 1L-MoS_2 is restricted to the domain wall surfaces, generating deterministic p-n regions on 1L-MoS_2 with exceptional precision. The ultra-narrow MoS_2 p-n junctions display a clear rectifying diode like behavior opening new routes for the design of simple and cost-effective electronic and optoelectronic devices based on the integration of 1L-MoS_2 with domain engineered ferroelectric crystals. Finally, by using all optical methods we have also shown the possibility of locally modifying the potential barrier height between consecutive p-n junctions. We demonstrate that tuning the amount of photodoping in the system enables changing the strength of the in-built electric field at consecutive junctions, leading to a switchable spatial redistribution of the emitted PL with the laser scanning direction. The spatial hysteresis behavior observed in the spontaneous emission envisages the possibility of reversibly switching the photocurrent direction in photovoltaic architectures based thus providing alternative pathways for the realization of novel electrically and optically driven low dimensional-based optoelectronic devices. All in one, our results point out different light-matter interaction processes taking place in 2D materials on ferroelectric substrates and open up prospects for unraveling new physical phenomena and search for innovative nanodevices harnessing the surface selectivity provided by ferroelectric domain engineered structures.

4. Experimental Section

Sample Preparation and Characterization: Mechanically exfoliated MoS_2 flakes from a bulk crystal were deposited onto a polydimethylsiloxane sheet and deterministically transferred[53] to the polar surface of commercially available (Covesion) periodically poled lithium niobate crystals. The ferroelectric domain patterns were fabricated by electric field poling on a 0.5 mm thick $LiNbO_3$ crystal. To ensure a proper spatial resolution during the optical measurements, the period of the alternate structure was

close to 20 µm (domain width ≈11 µm). The number of layers of the MoS_2 flakes was determined by means of differential micro-reflectance experiments in the 400–900 nm spectral range. To that end, the light from a halogen lamp was focused and collected through a 100× microscope objective (N.A. = 0.95) and directed to an optical fiber coupled to a CCD spectrometer (Spectral Products CVI SM440). A spatial pinhole was employed to further improve the spatial resolution (≈1 µm).

Photoluminescence Measurements: Spatially resolved micro-PL experiments were performed with a customized laser scanning confocal microscope (Olympus BX41) provided with a two-axis XY motorized platform with 0.3 µm spatial resolution. An Ar^+ laser (Spectra Physics Model 177-Series) with a filtered emission at 488 nm was used as excitation source. The pump beam was focused onto the surface sample by a 100× microscope objective (N.A. = 0.9). The diameter of the excitation spot was ≈1 µm. The PL signal was collected in backscattering geometry with the same objective lens and directed by an optical fiber to a Peltier-cooled Horiba Synapse CCD connected to a Horiba iHR 550 monochromator. A notch filter at 488 nm was employed to suppress the reflected laser beam from the collected signal.

Electrical Characterization: The electrical characterization was carried out by means of a home-built two-terminal probe station with 2 sets of xyz piezomotors that allow precise positioning of the electrical probes. These were conductive AFM tips that protrude from the very end of the cantilever (Nanosensors ATEC-EFM) with a nominal stiffness of 2.8 N m^{-1}, ensuring real tip visibility from above for a soft and accurate mechanical and electrical contact. To characterize the electrical properties of the system, the probes were brought into direct contact with the MoS_2 flakes (see Figure 3c), as verified using a force sensor with a sensitivity of ≈1 mN located underneath the sample. This ensures a good electrical contact between the probes and the MoS_2.[54] The experimental set up includes a Keithley 2400 source meter to apply the bias voltage between electrodes, a Femto DLPCA-200 variable-gain low-noise current preamplifier, and a Keithley 2000 multimeter to measure the output of the preamplifier.

Supporting Information

Supporting Information is available from the Wiley Online Library or from the author.

Acknowledgements

M.O.R., D.H.P., and L.E.B. acknowledge funding from the Spanish State Research Agency MICIU/AEI/10.13039/501100011033 under grants PID2019-108257GB-I00 and PID2022-137444NB-I00. P.A. acknowledges financial support from Comunidad de Madrid and Universidad Autónoma de Madrid (SI3-PJI-2021-00479), and from MICIU/AEI under grants TED2021-132219A-I00, PID2022-142331NB-I00, Ramón y Cajal fellowship RYC2020-030302-I, and "María de Maeztu" Programme for Units of Excellence in R&D (CEX2018-000805-M). P.M. acknowledges funding from the Spanish State Research Agency under grant PID2019-108257GB-I00 and from Comunidad de Madrid and Universidad Autónoma de Madrid (SI1-PJI-2019-001052020). J.G.H. acknowledges financial support from MICIU/AEI under grant PID2019-106268GB-C31 and PID2022-138908NB-C32.

Conflict of Interest

The authors declare no conflict of interest.

Data Availability Statement

The data that support the findings of this study are available from the corresponding author upon reasonable request.

Keywords

ferroelectrics, lithium niobate, monolayer MoS_2, photodoping, photoluminescence modulation, p-n homojunctions

Received: March 5, 2024
Revised: May 23, 2024
Published online:

[1] J. Jiang, Y. Wen, H. Wang, L. Yin, R. Cheng, C. Liu, L. Feng, J. He, *Adv. Electron. Mater.* **2021**, *7*, 2001125.
[2] B. W. H. Baugher, H. O. H. Churchill, Y. Yafang, P. Jarillo-Herrero, *Nat. Nanotechnol.* **2014**, *9*, 262.
[3] L. Cheng, J. Yu, Y. Wei, Z. Feng, Y. Li, Y. Wang, N. Xu, Z. L. Wang, Q. Sun, *Nano Energy* **2023**, *114*, 108632.
[4] A. Pospischil, M. M. Furchi, T. Mueller, *Nat. Nanotechnol.* **2014**, *9*, 257.
[5] J. S. Ross, P. Klement, A. M. Jones, N. J. Ghimire, J. Yan, D. G. Mandrus, T. Taniguchi, K. Watanabe, K. Kitamura, W. Yao, D. H. Cobden, X. Xu, *Nat. Nanotechnol.* **2014**, *9*, 268.
[6] X. Hong, J. Kim, S. F. Shi, Y. Zhang, C. Jin, Y. Sun, S. Tongay, J. Wu, Y. Zhang, F. Wang, *Nat. Nanotechnol.* **2014**, *9*, 682.
[7] R. Frisenda, A. J. Molina-Mendoza, T. Mueller, A. Castellanos-Gomez, H. S. J. van der Zant, *Chem. Soc. Rev.* **2018**, *47*, 3339.
[8] C. Huang, S. Wu, A. M. Sanchez, J. J. P. Peters, R. Beanland, J. S. Ross, P. Rivera, W. Yao, D. H. Cobden, X. Xu, *Nat. Mater.* **2014**, *13*, 1096.
[9] M. Y. Li, Y. Shi, C. C. Cheng, L. S. Lu, Y. C. Lin, H. L. Tang, M. L. Tsai, C. W. Chu, K. H. Wei, J. H. He, W. H. Chang, K. Suenaga, L. J. Li, *Science* **2015**, *349*, 524.
[10] X. Liu, Q. Wu, M. Dai, Q. Xu, X. Zhang, Z. Cai, K. K. Ostrikov, X. Gu, H. Nan, S. Xiao, *ACS Appl. Electron. Mater.* **2023**, *5*, 5494.
[11] F. Wang, K. Pei, Y. Li, H. Li, T. Zhai, *Adv. Mater.* **2021**, *33*, 2005303.
[12] Z. Q. Xu, Y. Zhang, Z. Wang, Y. Shen, W. Huang, X. Xia, W. Yu, Y. Xue, L. Sun, C. Zheng, *2D Mater.* **2016**, *3*, 041001.
[13] H. Xia, M. Luo, W. Wang, H. Wang, T. Li, Z. Wang, H. Xu, Y. Chen, Y. Zhou, F. Wang, R. Xie, P. Wang, W. Hu, W. Lu, *Light. Sci. Appl.* **2022**, *11*, 170.
[14] S. Mouri, Y. Miyauchi, K. Matsuda, *Nano Lett.* **2013**, *13*, 5944.
[15] M. S. Choi, D. Qu, D. Lee, X. Liu, K. Watanabe, T. Taniguchi, W. J. Yoo, *ACS Nano* **2014**, *8*, 9332.
[16] H. M. Li, D. Lee, D. Qu, X. Liu, J. Ryu, A. Seabaugh, W. J. Yoo, *Nat. Commun.* **2015**, *6*, 6564.
[17] T. Jin, J. Mao, J. Gao, C. Han, K. P. Loh, A. T. S. Wee, W. Chen, *ACS Nano* **2022**, *16*, 13595.
[18] L. Jin, H. Wang, R. Cao, K. Khan, A. K. Tareen, S. Wageh, A. A. Al-Ghamdi, S. Li, D. Li, Y. Zhang, H. Zhang, *APL Mater.* **2022**, *10*, 060903.
[19] S. Puebla, T. Pucher, V. Rouco, G. Sanchez-Santolino, Y. Xie, V. Zamora, F. A. Cuellar, F. J. Mompean, C. Leon, J. O. Island, M. Garcia-Hernandez, J. Santamaria, C. Munuera, A. Castellanos-Gomez, *Nano Lett.* **2022**, *22*, 7457.
[20] L. Lv, F. Zhuge, F. Xie, X. Xiong, Q. Zhang, N. Zhang, Y. Huang, T. Zhai, *Nat. Commun.* **2019**, *10*, 3331.
[21] G. Wu, X. Wang, Y. Chen, S. Wu, B. Wu, Y. Jiang, H. Shen, T. Lin, Q. Liu, X. Wang, P. Zhou, S. Zhang, W. Hu, X. Meng, J. Chu, J. Wang, *Adv. Mater.* **2020**, *32*, 1907937.
[22] B. Wen, Y. Zhu, D. Yudistira, A. Boes, L. Zhang, T. Yidirim, B. Liu, H. Yan, X. Sun, Y. Zhou, Y. Xue, Y. Zhang, L. Fu, A. Mitchell, H. Zhang, Y. Lu, *ACS Nano* **2019**, *13*, 5335.
[23] P. Soubelet, J. Klein, J. Wierzbowski, R. Silvioli, F. Sigger, A. V. Stier, K. Gallo, J. J. Finley, *Nano Lett.* **2021**, *21*, 959.

[24] E. M. Alexeev, N. Mullin, P. Ares, H. Nevison-Andrews, O. Skrypka, T. Godde, A. Kozikov, L. Hague, Y. Wang, K. S. Novoselov, L. Fumagalli, J. K. Hobbs, A. I. Tartakovskii, *ACS Nano* **2020**, *14*, 11110.
[25] R. Kappera, D. Voiry, S. E. Yalcin, B. Branch, G. Gupta, A. D. Mohite, M. Chhowalla, *Nat. Mater.* **2014**, *13*, 1128.
[26] A. Allain, J. Kang, K. Banerjee, A. Kis, *Nat. Mater.* **2015**, *14*, 1195.
[27] P. Shen, C. Su, Y. Lin, A.-S. Chou, C. Cheng, J. H. Park, M. Chiu, A. Lu, H. Tang, M. M. Tavakoli, G. Pitner, X. Ji, Z. Cai, N. Mao, J. Wang, V. Tung, J. Li, J. Bokor, A. Zettl, C. Wu, T. Palacios, L. J. Li, J. Kong, *Nature* **2021**, *593*, 211.
[28] D. Zhu, L. Shao, M. Yu, R. Cheng, B. Desiatov, C. J. Xin, Y. Hu, J. Holzgrafe, S. Ghosh, A. Shams-Ansari, E. Puma, N. Sinclair, C. Reimer, M. Zhang, M. Lončar, *Adv. Opt. Photon.* **2021**, *13*, 242.
[29] A. Boes, L. Chang, C. Langrock, M. Yu, M. Zhang, Q. Lin, M. Lončar, M. Fejer, J. Bowers, A. Mitchell, *Science* **2023**, *379*, eabj4396.
[30] E. Preciado, F. J. R. Schülein, A. E. Nguyen, D. Barroso, M. Isarraraz, G. von Son, I. H. Lu, W. Michailow, B. Möller, V. Klee, J. Mann, A. Wixforth, L. Bartels, H. J. Krenner, *Nat. Commun.* **2015**, *6*, 8593.
[31] M. O. Ramírez, P. Molina, D. Hernández-Pinilla, G. López-Polín, P. Ares, L. Lozano-Martín, H. Yan, Y. Wang, S. Sarkar, J. Shuhaib, F. Leardini, J. Gómez-Herrero, M. Chhowalla, L. E. Bausá, *Laser Photonics Rev.* **2024**, *18*, 2300817.
[32] C. Baeumer, D. Saldana-Greco, J. M. P. Martirez, A. M. Rappe, M. Shim, L. W. Martin, *Nat. Commun.* **2015**, *6*, 6136.
[33] X. Liang, H. Guan, K. Luo, Z. He, A. Liang, W. Zhang, Q. Lin, Z. Yang, H. Zhang, C. Xu, H. Xie, F. Liu, F. Ma, T. Yang, H. Lu, *Laser Photonics Rev.* **2023**, *17*, 2300286.
[34] H. Y. Guan, J. Y. Hong, X. L. Wang, J. Y. Ming, Z. L. Zhang, A. J. Liang, X. Y. Han, J. L. Dong, W. T. Qiu, Z. Chen, H. H. Lu, H. Zhang, *Adv. Optical Mater.* **2021**, *9*, 2100245.
[35] S. V. Kalinin, D. A. Bonnell, *Phys. Rev. B* **2001**, *63*, 125411.
[36] J. N. Hanson, B. J. Rodriguez, R. J. Nemanich, A. Gruverman, *Nanotechnology* **2006**, *17*, 4946.
[37] K. P. Dhakal, D. L. Duong, J. Lee, H. Nam, M. Kim, M. Kan, Y. H. Lee, J. Kim, *Nanoscale* **2014**, *6*, 13028.
[38] Y. Niu, S. Gonzalez-Abad, R. Frisenda, P. Marauhn, M. Drüppel, P. Gant, R. Schmidt, N. S. Taghavi, D. Barcons, A. J. Molina-Mendoza, S. M. de Vasconcellos, R. Bratschitsch, D. P. de Lara, M. Rohlfing, A. Castellanos-Gómez, *Nanomater.* **2018**, *8*, 725.
[39] S. M. Shinde, K. P. Dhakal, X. Chen, W. S. Yun, J. D. Lee, H. Kim, J.-H. Ahn, *NPG Asia Mater* **2018**, *10*, e468.
[40] A. Arora, K. Nogajewski, M. Molas, M. Koperski, M. Potemski, *Nanoscale* **2015**, *7*, 20769.
[41] M. Amani, D. H. Lien, D. Kiriya, J. Xiao, A. Azcatl, J. Noh, S. R. Madhvapathy, R. Addou, K. S. KC, M. Dubey, K. Cho, R. M. Wallace, S. C. Lee, J. H. He, J. W. Ager III, X. Zhang, E. Yablonovitch, A. Javey, *Science* **2015**, *350*, 1065.
[42] K. F. Mak, K. He, C. Lee, G. H. Lee, J. Hone, T. F. Heinz, J. Shan, *Nat. Mater.* **2013**, *12*, 207.
[43] P. Wang, J. Wang, Y. Zheng, H. Shi, X. Sun, W. Liu, B. Gao, *Phys. Chem. Chem. Phys.* **2021**, *23*, 17265.
[44] N. Lundt, E. Cherotchenko, O. Iff, X. Fan, Y. Shen, P. Bigenwald, A. V. Kavokin, S. Höfling, C. Schneider, *Appl. Phys. Lett.* **2018**, *112*, 031107.
[45] F. Cadiz, C. Robert, G. Wang, W. Kong, X. Fan, M. Blei, D. Lagarde, M. Gay, M. Manca, T. Taniguchi, K. Watanabe, T. Amand, X. Marie, P. Renucci, S. Tongay, B. Urbaszek, *2D Mater.* **2016**, *3*, 045008.
[46] Y. Sun, R. J. Nemanich, *J. Appl. Phys.* **2011**, *109*, 104302.
[47] R. Soklaski, Y. Liang, L. Yang, *Appl. Phys. Lett.* **2014**, *104*, 193110.
[48] S. V. Kalinin, D. A. Bonnell, T. Alvarez, X. J. Lei, Z. H. Hu, R. Shao, J. H. Ferris, *Adv. Mater.* **2004**, *16*, 795.
[49] M. O. Ramírez, P. Molina, A. Gómez-Tornero, D. Hernández-Pinilla, L. Sánchez-García, S. Carretero, L. E. Bausá, *Adv. Mater.* **2019**, *31*, 1901428.
[50] A. Kakekhani, S. Ismail-Beigi, E. I. Altman, *Surf. Sci.* **2016**, *650*, 302.
[51] E. Yraola, P. Molina, J. L. Plaza, M. O. Ramírez, L. E. Bausá, *Adv. Mater.* **2013**, *25*, 910.
[52] H. Yamaguchi, J.-C. Blancon, R. Kappera, S. Lei, S. Najmaei, B. D. Mangum, G. Gupta, P. M. Ajayan, J. Lou, M. Chhowalla, J. J. Crochet, A. D. Mohite, *ACS Nano* **2015**, *9*, 840.
[53] A. Castellanos-Gómez, M. Buscema, R. Molenaar, V. Singh, L. Janssen, H. S. J. van der Zant, G. A. Steele, *2D Mater.* **2014**, *1*, 011002.
[54] Y. Manzanares-Negro, J. Quan, M. Rassekh, M. Moaied, X. Li, P. Ares, J. J. Palacios, J. Gomez-Herrero, C. Gomez-Navarro, *2D Mater.* **2023**, *10*, 021003.